AGU PUBLICATIONS

JGR

Journal of Geophysical Research: Atmospheres

RESEARCH ARTICLE
10.1002/2014JD022940

Key Points:
- Deepening ASL in Ross Sea influences warming of western West Antarctica
- Increasing South Atlantic pressure influencing western Antarctic Peninsula warming
- ENSO linked to South Atlantic/Peninsula; PDO linked to ASL/West Antarctica

Correspondence to:
K. R. Clem,
kyle.clem@vuw.ac.nz

Citation:
Clem, K. R., and R. L. Fogt (2015), South Pacific circulation changes and their connection to the tropics and regional Antarctic warming in austral spring, 1979–2012, *J. Geophys. Res. Atmos.*, *120*, 2773–2792, doi:10.1002/2014JD022940.

Received 2 DEC 2014
Accepted 7 MAR 2015
Accepted article online 11 MAR 2015
Published online 13 APR 2015

South Pacific circulation changes and their connection to the tropics and regional Antarctic warming in austral spring, 1979–2012

Kyle R. Clem[1] and Ryan L. Fogt[2]

[1]School of Geography, Environment and Earth Sciences, Victoria University of Wellington, Wellington, New Zealand, [2]Department of Geography, Ohio University, Athens, Ohio, USA

Abstract After 1979, statistically significant warming in Antarctica is only observed in austral spring (September–November, SON) across West Antarctica and the Antarctic Peninsula. While previous work has linked this warming to reductions in sea ice cover, we note that a substantial (30–60%) portion of the warming is related to changes in the SON atmospheric circulation. In particular, western Antarctic Peninsula warming is consistent with increasing pressure in the South Atlantic, while western West Antarctica warming is tied to a deepening of the Amundsen Sea low near the eastern Ross Sea. While both of these circulation changes are associated with increased warm, northerly flow toward the Antarctic continent, they are connected with different aspects of tropical variability. The increase in pressure in the South Atlantic is associated with a trend toward more La Niña-like conditions in the tropical Pacific, and an associated Rossby wave train. In contrast, the deepening of the Amundsen Sea low is more strongly tied to a shift in the Pacific Decadal Oscillation (PDO) toward its negative phase since the 1990s. Compared to typical La Niña events, the recent negative PDO events display a different tropical forcing, which drives a Rossby wave train that propagates more meridionally across the South Pacific, culminating in the eastern Ross Sea, rather than in the South Atlantic. The results suggest multiple independent forcing mechanisms governing the SON pressure trends and associated Antarctic Peninsula and West Antarctica warming after 1979, which partially cancel each other out in the Amundsen Sea and portions of eastern West Antarctica.

1. Introduction

An increasing number of observation-based [*Turner et al*., 2005] and reconstruction-based [*Chapman and Walsh*, 2007; *Monaghan et al*., 2008; *Steig et al*., 2009; *O'Donnell et al*., 2011; *Bromwich et al*., 2013, 2014; *Nicolas and Bromwich*, 2014] studies point to statistically significant warming across the Antarctic Peninsula and West Antarctica since the 1957–1958 International Geophysical Year. These studies agree on a regional and seasonal nature to the trends, namely that warming trends are primarily insignificant across most of East Antarctica in all seasons, and strongest across the Antarctic Peninsula in austral winter and throughout all of West Antarctica during austral spring (September–November; SON hereafter). Furthermore, there is a time dependency on the level of statistical significance; only in SON are temperature trends across both West Antarctica and the western Antarctic Peninsula significant after 1979 [*Schneider et al*., 2012; *Bromwich et al*., 2013; *Nicolas and Bromwich*, 2014].

There are a few suggestions on the causality of the Antarctic temperature trends in austral winter. A number of studies suggest that the temperature trends are linked to changes in the sea ice concentrations, especially a decrease in the Bellingshausen Sea [*King*, 1994; *Jacobs and Comiso*, 1997; *Meredith and King*, 2005; *Turner et al*., 2005]. In particular, the warming along the Antarctic Peninsula in austral winter is at least partly related to the extent of open water west of the peninsula, leading to strong warming rates at Faraday station in winter. The changes in the regional ice-ocean properties are consistent with trends in the atmospheric circulation, which displays a deepening of the Amundsen Sea low in austral autumn [*Holland and Kwok*, 2012; *Turner et al*., 2013]. Changes in sea ice concentration and extent are strongly linked to the meridional wind associated with this feature [*Holland and Kwok*, 2012], and a study by *Ding and Steig* [2013] note that the decreases in sea ice concentration along the western Antarctic Peninsula associated with the deepening of the Amundsen Sea low in austral autumn persist through SON and are consistent with the warming across the western Peninsula. However, earlier work by *Ding et al*. [2011] show that in winter, the regional

atmospheric circulation trends in the Amundsen Sea low are linked to the central tropical Pacific sea surface temperatures (SSTs) in a different fashion. According to *Ding et al*. [2011], increasing SSTs in the central tropical Pacific generate a Rossby wave train similar in style to the Pacific-South American (PSA) [*Mo and Higgins*, 1998] pattern that produces positive geopotential height anomalies in the Amundsen Sea in winter, driving increased warm air advection onto West Antarctica on its western flank. This scenario would be associated with cooling and wind-driven increases in sea ice along the western Antarctic Peninsula in winter, contrary to the observed warming and decreases in sea ice extent there [*Vaughan et al*., 2003; *Turner et al*., 2005; *Stammerjohn et al*., 2008, 2012]. Therefore, the high southern latitude regional circulation changes associated with tropical Pacific SST anomalies are not fully understood, especially with regard to the warming along the western Peninsula. Adding to this complexity, a recent study by *Li et al*. [2014] suggests that warming in the tropical Atlantic also drives a Rossby wave train, which propagates from the South Atlantic across the Southern Ocean, eventually arriving in the Amundsen and Bellingshausen Seas. In this scenario, negative pressure anomalies are observed in the Amundsen Sea region during winter, which is consistent with the warming along the Antarctic Peninsula, and the sea ice extent decreases in the Bellingshausen Sea and increases in the Ross Sea regions but is inconsistent with the work of *Ding et al*. [2011] who point at increasing pressure anomalies in the Amundsen Sea during winter.

Despite SON being the season of strongest and most persistent warming across portions of Antarctica, even less is known on the causality of the temperature changes compared to winter. *Schneider et al*. [2012] suggest that the warming across West Antarctica during SON is strongly correlated ($r = -0.73$) to the sea ice area in the Amundsen-Bellingshausen Seas, also suggested by *Ding and Steig* [2013]. The decrease in sea ice in this region is linearly congruent to nearly half of the warming trends across West Antarctica. Using climate model simulations and empirical orthogonal functions of the SON atmospheric circulation at 850 hPa, *Schneider et al*. [2012] noted that changes in the atmospheric circulation during SON, consistent with both the warming across West Antarctica and the regional sea ice changes in the Amundsen and Bellingshausen Seas, are similarly linked to tropical activity. They find a strong warming trend in SSTs along the western tropical Pacific ocean extending southeastward along the South Pacific convergence zone, which they suggest forces a Rossby wave train to the high-latitude South Pacific reminiscent of the PSA pattern that *Ding et al*. [2011] connected to the warming trends in austral winter across West Antarctica. Importantly, *Schneider et al*. [2012] find negative geopotential height trends in the high-latitude South Pacific to be associated with the SON warming in West Antarctica, while *Ding et al*. [2011] found positive geopotential height trends to be associated with winter warming in West Antarctica.

This study builds upon the work of *Schneider et al*. [2012] and *Ding and Steig* [2013] by further examining the Southern Hemisphere atmospheric circulation trends and their linkages to tropical activity and the regional Antarctic warming. We provide new statistical analyses that highlight distinct aspects of tropical variability that influence West Antarctica and the Antarctic Peninsula differently during SON. The paper is outlined as follows: data and methods are discussed in section 2, and our results, beginning with a justification for focusing solely on austral spring, are provided in section 3. A summary and conclusions are offered in section 4.

2. Data and Methods

2.1. Data Employed

El Niño–Southern Oscillation (ENSO) activity is primarily monitored using the Southern Oscillation Index (SOI) obtained from the Climate Prediction Center (www.cpc.noaa.gov); the Niño 3.4 region (5°N–5°S, 170°–120°W) and Niño 1 + 2 region (0°–10°S, 90°–80°W) SST anomalies are also employed. For Southern Annular Mode (SAM) events, we use the observation-based index of *Marshall* [2003]. We also employ the monthly Pacific Decadal Oscillation (PDO) index from the Joint Institute for the Study of the Atmosphere and Ocean, available online (http://jisao.washington.edu/pdo/PDO.latest) [*Mantua et al*., 1997; *Zhang et al*., 1997].

For Antarctic Peninsula meteorological data, we use the quality-controlled online Reference Antarctic Data for Environmental Research archive [*Turner et al*., 2004] at five stations with nearly complete records spanning over 30 years. For temperature observations in interior West Antarctica, we use the patched and recently corrected record at Byrd station from *Bromwich et al*. [2013, 2014].

Table 1. Seasonal Trends and 95% Confidence Intervals for *Marshall* [2003] SAM Index, SOI, PDO, and PDO_Residual (Units of Standardized Index Decade^{-1}), Niño 3.4 and 1+2 SST Anomalies (Units of °C Decade^{-1}), Antarctic Peninsula Station Temperatures, Byrd Reconstructed Temperatures, and West Antarctic ERA-Interim 2 m Temperatures (Units of °C Decade^{-1})[a]

	DJF		MAM		JJA		SON	
	1957–2012	1979–2012	1957–2012	1979–2012	1957–2012	1979–2012	1957–2012	1979–2012
Climate Modes								
SAM index	**0.35 ± 0.21***	**0.48 ± 0.40**	**0.25 ± 0.17***	**0.31 ± 0.36**	0.15 ± 0.20	0.11 ± 0.42	0.07 ± 0.19	0.05 ± 0.44
SOI	0.12 ± 0.30	**0.64 ± 0.67**	−0.06 ± 0.19	0.33 ± 0.41	−0.07 ± 0.18	0.09 ± 0.40	0.08 ± 0.23	**0.49 ± 0.47**
Niño SST 3.4	−0.04 ± 0.17	−0.2 ± 0.38	0.02 ± 0.10	−0.08 ± 0.21	0.04 ± 0.11	0.02 ± 0.23	0.04 ± 0.16	−0.04 ± 0.34
Niño SST 1 + 2	0.09 ± 0.14	−0.03 ± 0.33	0.09 ± 0.17	−0.01 ± 0.39	0.10 ± 0.19	−0.03 ± 0.42	0.07 ± 0.17	−0.17 ± 0.38
PDO	0.07 ± 0.16	**−0.36 ± 0.31**	0.13 ± 0.16	**−0.47 ± 0.29***	0.04 ± 0.16	**−0.52 ± 0.34***	−0.06 ± 0.16	**−0.60 ± 0.30***
PDO_residual	0.10 ± 0.14	−0.21 ± 0.28	0.10 ± 0.14	**−0.34 ± 0.26**	0.02 ± 0.15	**−0.49 ± 0.31***	−0.03 ± 0.13	**−0.40 ± 0.27***
Antarctic Peninsula Temperatures								
Faraday	**0.23 ± 0.10***	0.15 ± 0.22	**0.47 ± 0.22***	**0.37 ± 0.30**	**1.22 ± 0.43***	**1.18 ± 0.85***	**0.42 ± 0.24***	**0.76 ± 0.48***
Rothera	0.13 ± 0.18	0.04 ± 0.18	**0.66 ± 0.41***	**0.61 ± 0.46**	**1.06 ± 0.91**	**0.88 ± 1.01**	**0.79 ± 0.52***	**0.61 ± 0.54**
Bellingshausen	0.06 ± 0.11	−0.09 ± 0.18	**0.27 ± 0.24**	0.20 ± 0.37	0.33 ± 0.44	0.12 ± 0.71	0.04 ± 0.21	0.16 ± 0.34
Esperanza	**0.34 ± 0.13***	**0.25 ± 0.26**	**0.38 ± 0.35**	0.16 ± 0.76	**0.35 ± 0.36**	−0.21 ± 0.81	0.15 ± 0.26	0.36 ± 0.62
Marambio	**0.42 ± 0.22***	**0.39 ± 0.35**	0.49 ± 0.64	0.35 ± 0.95	0.27 ± 0.68	−0.24 ± 0.95	0.22 ± 0.47	0.41 ± 0.73
West Antarctic Temperatures								
Byrd	0.15 ± 0.21	0.20 ± 0.43	0.28 ± 0.35	0.18 ± 0.86	**0.49 ± 0.43**	0.54 ± 1.03	**0.63 ± 0.32***	**0.59 ± 0.71**
All West Antarctica		−0.04 ± 0.26		−0.01 ± 0.55		0.43 ± 0.71		0.31 ± 0.47
Western West Antarctica		0.00 ± 0.30		0.02 ± 0.79		0.78 ± 1.02		**0.63 ± 0.56**
Eastern West Antarctica		−0.09 ± 0.27		−0.05 ± 0.40		0.08 ± 0.60		−0.00 ± 0.47

[a]Here the West Antarctic regions are defined as in Figure 1 within 72°S–85.5°S, and over the following range of longitudes: All West Antarctica (75°W–156°W), eastern West Antarctica (75°W–115.5°W), and western West Antarctica (115.5°W–156°W). Trends are calculated from 1957 or the start of the record, ending at 2012 (first column), and over the period 1979–2012 (second column). Boldface trends are significantly different from zero at $p < 0.10$, boldface and underlined trends are significantly different from zero at $p < 0.05$, and trends significantly different from zero at $p < 0.01$ are boldface and underlined and further denoted with an asterisk. Temperature data for Rothera, Bellingshausen, and Marambio start in 1977, 1968, and 1970, respectively; otherwise, the long-term trends are from 1957.

Several fields from the European Centre for Medium-Range Weather Forecasts (ECMWF) Interim reanalysis (hereafter ERA-Interim) [*Dee et al*., 2011] at 1.5°× 1.5° latitude-longitude resolution are also employed, starting in 1979. Although previous work suggests that ERA-Interim best reproduces the Southern Hemisphere atmospheric circulation at high southern latitudes [*Bromwich et al*., 2011; *Bracegirdle and Marshall*, 2012], near-surface temperature results from ERA-Interim are validated using three other contemporary reanalyses: the National Centers for Environmental Prediction (NCEP) Climate Forecast System Reanalysis (CFSR) [*Saha et al*., 2010], the National Aeronautic and Space Administration (NASA) Modern-Era Retrospective Analysis for Research and Applications (MERRA) [*Rienecker et al*., 2011], and the Japanese 55 year Reanalysis (JRA-55) [*Kobayashi et al*., 2015]. We also make use of the monthly National Oceanic and Atmospheric Administration (NOAA) Optimum interpolated (OI) SST data set, version 2 [*Reynolds et al*., 2002], available from NOAA's Earth System Research Laboratory (http://www.esrl.noaa.gov/psd/data/gridded/data.noaa.oisst.v2.html). These data are at a 1°× 1° latitude-longitude resolution starting in 1981. For sea ice concentrations, we follow *Ding and Steig* [2013] and use the Hadley Centre Sea Ice and Sea Surface Temperature data set (HadISST), also at 1°× 1° latitude-longitude resolution [*Rayner et al*., 2003].

2.2. Methods

We employ linear regression, linear congruency, correlation, and anomaly composite analyses to investigate the relationships between the climate and regional atmospheric circulation. Significance of the composite anomalies as well as the correlation and regression coefficients is calculated following a Student's two-tailed *t* test. For all analyses, the primary period of study is from 1979 to 2012, with the climatological reference period defined as 1981–2010; however, some linear relationships are calculated back further in time as the observational records allow. Seasons are defined with respect to the Southern Hemisphere: austral summer (December–February, DJF), austral autumn (March–May, MAM), austral winter (June–August, JJA), and austral spring (September–November, SON).

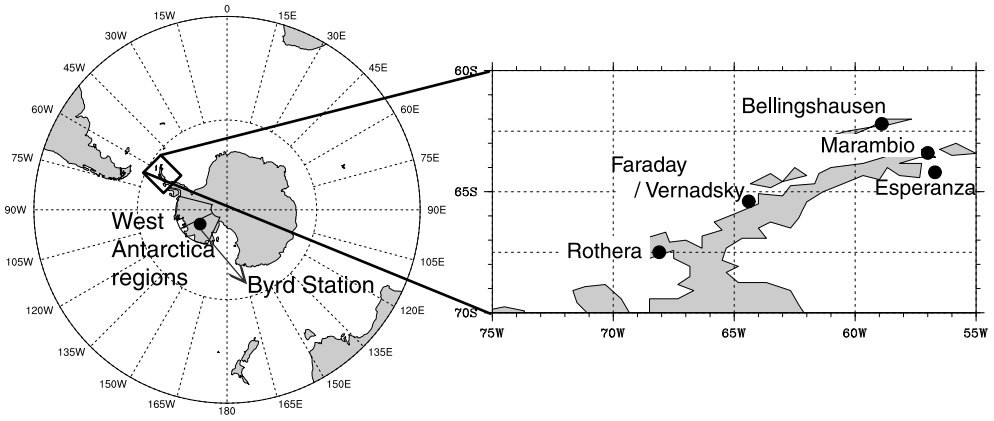

Figure 1. Map showing the locations of the West Antarctica regions, Byrd Station, and the Antarctic Peninsula stations used in the study.

3. Results

3.1. Seasonal Trends

As previously discussed, there are several ongoing statistically significant trends in the regional Antarctic climate, which vary temporally and seasonally. These trends along with trends in various relevant modes of climate variability are presented in Table 1. Seasonal least squares linear regression coefficients are calculated over time (trends) for the following: station temperature data on the Antarctic Peninsula, *Bromwich et al*. [2013, 2014] Byrd reconstructed temperature data, and ERA-Interim 2m temperature data over West Antarctica in three separate area-averaged regions between 72°S and 85.5°S: all of West Antarctica (75°W–156°W), eastern West Antarctica (75°W–115.5°W), and western West Antarctica (115.5°W–156°W). Further justification for these geographical regions will be given later when the ERA-Interim spatial temperature trends are investigated; a slightly different region in western West Antarctica will also be investigated. Figure 1 displays the locations of the regions and station data used in the study. For trends in climate modes, seasonal linear trends are also calculated for the *Marshall* [2003] SAM index, the SOI, the Niño 3.4 and 1+2 SST anomalies, and the PDO index. Seasonal trends over the 1957–2012 (or since the start of the record if after 1957), as well as from 1979 to 2012, are displayed in Table 1.

Looking first at the temperature trends since 1957 (Table 1), there are significant ($p < 0.01$) warming trends observed across the northeast Antarctic Peninsula (i.e., Esperanza and Marambio) during DJF, which coincide with significant ($p < 0.01$) positive trends in the SAM index. In its positive phase, the SAM describes low-pressure/geopotential height anomalies poleward of 60°S, and high-pressure/geopotential height anomalies in the midlatitudes, near 45°S [*Thompson et al*., 2000; *Marshall*, 2003]. As noted previously [i.e., *Marshall et al*., 2006; *Orr et al*., 2008], the summer positive SAM index trends lead to warming along the northeast Peninsula mainly through adiabatic warming of air parcels descending on the lee of the mountains across the Antarctic Peninsula. The positive trends in the SAM index continue into MAM, as do the positive temperature trends along the northeast Peninsula at Esperanza, albeit not as significant as in DJF. The positive SAM index trends and northeast Peninsula warming trends are present over both the 1957–2012 period and after 1979 in DJF, and there are no other persistent trends throughout both these periods in DJF. A nearly ubiquitous warming is noted across the peninsula during MAM, which *Ding and Steig* [2013] attribute to a deepening of the Amundsen Sea low and a reduction of sea ice off the west coast of the Antarctic Peninsula. This warming is persistent over both time periods across the western Antarctic Peninsula (i.e., Faraday and Rothera) only. Despite the warming across the peninsula during DJF and MAM, there are no significant trends in the ERA-Interim West Antarctic 2m temperatures or at Byrd during these two seasons.

Turning to JJA and SON, the positive trends in the SAM weaken and are no longer statistically significant; similarly, the positive temperature trends on the northeast Antarctic Peninsula weaken and are no longer significant. Meanwhile, statistically significant ($p < 0.01$) warming trends are observed along the western Antarctic Peninsula (i.e., Faraday and Rothera) during JJA and SON, which *Ding and Steig* [2013] attribute to a persistent reduction in sea ice concentration off the west coast of the Antarctic Peninsula stemming from the

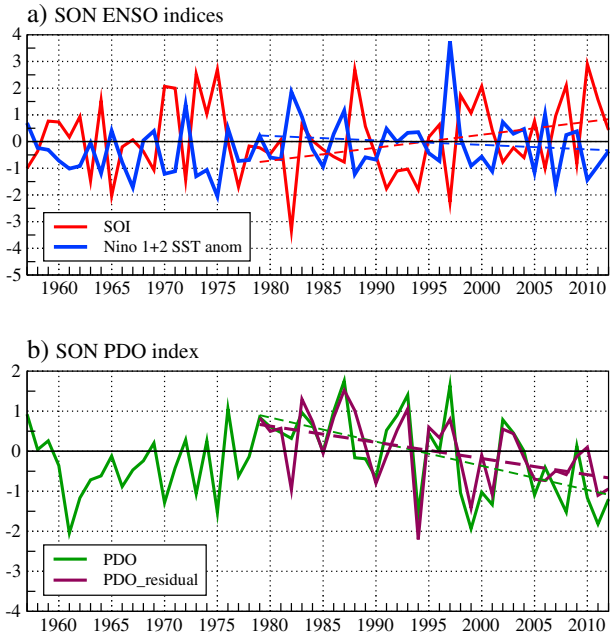

Figure 2. Time series of SON (a) SOI and Niño 1 + 2 SST anomalies and (b) PDO index and the PDO_residual index (after 1979). Also plotted are the trends in the time series from 1979 to 2012 with dashed lines.

changes induced in MAM. A significant warming trend is found at Byrd during JJA, and across western West Antarctica and Byrd during SON. The strongest warming trends on the western Peninsula are observed during JJA, while the strongest warming over West Antarctica is observed during SON. The warming over the western Peninsula remains strong and statistically significant over both time periods during JJA and SON, actually increasing in magnitude at Faraday from 1957 to 2012 to 1979–2012 during SON. Meanwhile, the strongest warming at Byrd during JJA and SON appears to be during the early part of the record, as the warming becomes statistically insignificant in JJA after 1979, and the significance decreases to $p < 0.10$ in SON after 1979, as confirmed across all West Antarctica by *Nicolas and Bromwich* [2014].

Based on ERA-Interim data, significant ($p < 0.05$) warming over the 1979–2012 period during SON is found only over the western half of West Antarctica. This suggests that significant warming over all of West Antarctica [*Steig et al.*, 2009; *O'Donnell et al.*, 2011; *Schneider et al.*, 2012; *Nicolas and Bromwich*, 2014] and at Byrd station [*Bromwich et al.*, 2013, 2014] was likely stronger before 1979. It is interesting that significant warming is observed only over the western half of West Antarctica after 1979 given that this area is geographically separated from the SON warming across the western Antarctic Peninsula. The regional disparity of the warming trends points to the likelihood that there are different regional atmospheric circulation changes (rather than a uniform change across all of the West Antarctic region) giving rise to the spatial pattern of SON warming implied in Table 1. Understanding these differences, which really are only occurring in SON, and their connection to circulation changes, large-scale modes of climate variability, and previous work [i.e., *Schneider et al.*, 2012; *Ding and Steig*, 2013] is the primary focus for the remainder of our analysis.

During SON, there are also changes in the tropical Pacific after 1979 (Table 1). In particular, a significant positive trend in the SOI is observed ($p < 0.05$) as is a significant negative trend in the PDO index ($p < 0.01$). To place the significant trends in the SOI and PDO index in context, the SON time series for both are displayed in Figure 2 along with the Niño 1 + 2 SST anomalies. The PDO index trend is negative (across all seasons, Table 1; not shown in Figure 2) reflecting the shift in this index from primarily positive values from the mid-1970s through mid-1990s to primarily negative values after 1998 (Figure 2b). During SON, the PDO trend over the 1979–2012 period is $-0.60\,\text{decade}^{-1}$, significantly different from zero at $p < 0.01$ (Table 1). Although the SOI trend since 1979 is sensitive to the negative value in 1982 (with the El Niño that year), the Niño 1 + 2 SST anomalies show a slight (insignificant) negative trend after 1979 (Table 1; dashed blue line in Figure 2a) indicating that the La Niña-like trend (from the SOI) is further supported by a cooling trend in the eastern tropical Pacific over the same period; it will be shown later that there are also statistically significant negative SST trends in SON in the eastern tropical Pacific during this period. Altogether, the trends in the SOI, Niño 1 + 2 SSTs, and PDO suggest a robust shift toward more La Niña-like conditions in the tropical Pacific after 1979 during SON.

Since the PDO index is partly related to ENSO variability (the correlation between the SON SOI and PDO index is −0.55, significant at $p < 0.01$), we created a PDO-ENSO residual index by linearly removing the ENSO component of the PDO. This was done by regressing the SOI on the PDO index over both the 1957–2012 and

Table 2. The 1979–2012 SON Temperature Trends (First Column, in Units of °C Decade^{-1}) and the Portion/Percentage (in Parentheses) of These Trends Linearly Congruent With the SOI (Second Column), PDO_Residual (Third Column), and MAM Sea Ice Near the Antarctic Peninsula (Final Column)[a]

	Temperature Trend	Congruent With SOI	Congruent With PDO_Residual	Congruent With MAM Antarctic Peninsula Sea Ice
Faraday	0.76	0.32 (*42.1%*)	0.06 (*7.9%*)	0.48 (*63.2%*)
Rothera	0.61	0.35 (*57.4%*)	0.09 (*14.8%*)	0.43 (*70.5%*)
Byrd	0.59	0.09 (*15.3%*)	0.17 (*28.8%*)	0.34 (*57.6%*)
All West Antarctica	0.31	0.03 (*9.7%*)	0.08 (*25.8%*)	0.13 (*41.9%*)
Western West Antarctica	0.63	−0.02 (*−3.2%*)	0.13 (*20.6%*)	0.22 (*34.9%*)

[a]The West Antarctic regions are defined as in Table 1.

1979–2012 time periods, using these relationships to predict the PDO index yearly for each period, and then subtracting this predicted PDO index (the part linearly related to the SOI) from the original PDO index. This newly formed PDO index is termed the PDO_residual, which has zero correlation with the SOI. PDO residual indices calculated using the various Niño SST anomalies are similar (not shown), with the residual PDO index based on the SOI displaying the weakest (but still significant) trend after 1979. Therefore, using the PDO residual index calculated from the SOI provides the most conservative estimate of how the PDO trend is independently (from ENSO) influencing the Southern Hemisphere climate. As discussed in prior work [*Zhang et al*., 1997; *Garreaud and Battisti*, 1999], the PDO_residual characterizes the low-frequency, decadal component of ENSO (ENSO-like interdecadal variability), although other factors besides ENSO influence the PDO [*Schneider and Cornuelle*, 2005]. The seasonal trends in the PDO_residual index are also given in Table 1, and the index and its SON trend after 1979 are also displayed in Figure 2b (note the PDO trends are stronger after the 1990s when the PDO began a shift toward its negative phase). Approximately 70% of the original (raw) interannual PDO variability is retained in the PDO_residual time series, indicating there is a substantial portion of the PDO index that operates linearly independent of the interannual ENSO variability. Furthermore, despite the PDO_residual trends being weaker than the raw PDO trends (reflecting the fact that a portion of the PDO trend is related to ENSO), both the PDO and PDO_residual trends are significant at $p < 0.01$ after 1979 during SON, indicating a robust shift in the PDO after the 1990s regardless of whether or not ENSO variability is retained. While there may be more persistent covariability leading to the similar trends in the SOI and PDO_residual index in Table 1, investigating this potential relationship/linkage is beyond the scope of our analysis. Regardless, our approach ensures that on interannual timescales the two indices are independent.

3.2. Atmospheric Circulation Trends and Their Connection to Antarctic Warming

Following *Ding and Steig* [2013], we examine the role of sea ice conditions off the coast of the Antarctic Peninsula from the HadISST data set. While *Ding and Steig* [2013] note a significant correlation between MAM sea ice that is related to tropical variability (through maximum covariance analysis), we note that the direct correlation of HadISST MAM-averaged sea ice near the Antarctic Peninsula (60°–75°S, 79.5°–52.5°W, as in *Ding and Steig* [2013]) is not statistically significant on detrended data during 1979–2012 ($r = -0.278$, $p > 0.10$), especially if autocorrelation of the sea ice time series is considered. This suggests that the trends contribute strongly to the covariance and dominate the linear relationships with the interannual variability at greater than 3 months lag. Further, *Ding and Steig* [2013] find stronger relationships with Antarctic Peninsula warming with a separate MAM sea ice index determined from maximum covariance analysis with tropical sea surface temperatures, rather than the actual/observed near-Peninsula MAM sea ice variability and SON Antarctic Peninsula temperatures. Therefore, the conclusion that MAM sea ice is related to the SON temperatures along the western Peninsula is somewhat misleading, as only a portion of the MAM sea ice variability is related to SON temperatures across the Antarctic Peninsula, and the relationship is only significant if the linear trends are retained.

The influence of the SON trends in the PDO_residual and the SOI on the SON temperature trends (from Table 1) is examined using linear congruency in Table 2. Linear congruency is calculated as in *Thompson et al*. [2000], by first calculating the trends in each variable/index, regressing the variable onto the climate index,

and multiplying the resulting regression coefficient by the linear trend of the climate index. Linear congruency therefore represents the portion of a trend in one variable (i.e., temperature) that would be expected from the trend in another variable (i.e., the SOI); thus, both variables must have a statistically significant trend for linear congruency analysis to be meaningful.

From Table 2, the MAM sea ice decreases are linearly congruent with more than 50% of the SON warming across the western Antarctic Peninsula (Faraday and Rothera) and over 30% of the SON warming across the western portion of West Antarctica, confirming the results of *Ding and Steig* [2013]. However, Table 2 demonstrates that the post-1979 positive trend in the SOI during SON is ~40–50% linearly congruent with the SON warming across the western Antarctic Peninsula, similar in magnitude to the MAM sea ice relationship. The strong SOI connection with western Peninsula temperatures in SON has also been discussed by *Clem and Fogt* [2013], supporting the idea that trends in the SOI would likely have a linear impact on western Peninsula climate. The SOI has a substantially weaker linear influence on the warming across West Antarctica: the positive trend in the SOI is congruent with only 10–15% of the warming at Byrd and across all of West Antarctica, and a weak cooling trend would be expected across western West Antarctica, contrary to the significant warming occurring there. Instead, the SON warming trends across West Antarctica are more linearly related to the negative trend in the PDO, with ~20–30% of the West Antarctic warming linearly congruent with the negative PDO_residual trend.

The differences between the warming across the western Antarctic Peninsula and western West Antarctica are better understood when looking spatially at atmospheric circulation trends. Figure 3 presents the 1979–2012 SON-averaged ERA-Interim mean sea level pressure (MSLP) and 10 m wind trends (Figure 3a) and 2 m temperature trends (Figure 3b), as well as the 1982–2012 SON-averaged SST trends (Figure 3c). The SON-averaged temperature trends across West Antarctica from other contemporary global reanalyses are presented in Figure 4. Figure 4 demonstrates that the significant warming across western West Antarctica found in ERA-Interim (discussed in Table 1 and in Figure 3b) is also found in the CFSR, JRA-55, and MERRA data sets. With the exception of JRA-55 (Figure 4c), which is an outlier and suggests significant warming has been occurring across all of West Antarctica, the CFSR and MERRA data sets suggest that the regionality of the West Antarctic warming is robust, and significant warming across West Antarctica is confined to western West Antarctica and the Ross Ice Shelf after 1979. The pattern of warming justifies the division of West Antarctica into eastern and western regions (Table 1 and Figure 1). The rate of warming here is also similar among reanalyses (Figure 4), with an average of ~0.6 ± 0.3°C decade^{-1} across western West Antarctica near the Ross Ice Shelf, consistent across all four reanalyses.

From Figure 3c, as alluded to earlier, significant negative trends in SSTs are observed near the west coast of tropical South America along with significant increases in SSTs across a large portion of the western tropical Pacific and the South Pacific convergence zone, giving credence to the robustness of the positive trend in the SOI (Figure 2a) toward increased La Niña-like conditions. These SST trends were also discussed in *Ding et al*. [2012] and reflect the trend toward the negative phase of the PDO [*Trenberth et al*., 2014].

In terms of the circulation trends, Figure 3a highlights two regions of statistically significant MSLP trends across the extratropical Southern Hemisphere: a negative pressure trend in the eastern Ross/western Amundsen Sea [*Fogt et al*., 2012; *Hosking et al*., 2013; *Turner et al*., 2013] and a positive pressure trend in the South Atlantic (significant at $p < 0.05$ and $p < 0.01$, respectively). Associated with these features is a significant increase in southerly flow in the Ross Sea and increases in northerly flow over the northern Antarctic Peninsula. The increased northerly flow across the Peninsula is consistent with the warming along the western Antarctic Peninsula over the 1979–2012 period (Tables 1, 2 and Figure 3b). Other contemporary reanalyses (CFSR, MERRA, and JRA-55) also show significant MSLP/wind trends in nearly identical regions as ERA-Interim (not shown), with the precise location and magnitude only varying slightly among data sets. Linear congruency was calculated over the 1979–2012 period between ERA-Interim area-averaged MSLP in the South Atlantic region that is trending positive (45°S–60°S, 45°W–15°W) and the temperature records at Faraday and Rothera (not shown). The increasing pressure in the South Atlantic is linearly congruent with more than 60% of the warming at Faraday, and more than 85% of the warming at Rothera, and therefore, the increasing pressure in the South Atlantic is consistent with more of the western Peninsula warming than any other mechanism presented so far.

Also of interest is the significant warming across western West Antarctica after 1979 during SON (Table 1 and Figures 3b and 4). Off the coast, winds are becoming more significantly easterly, associated with the

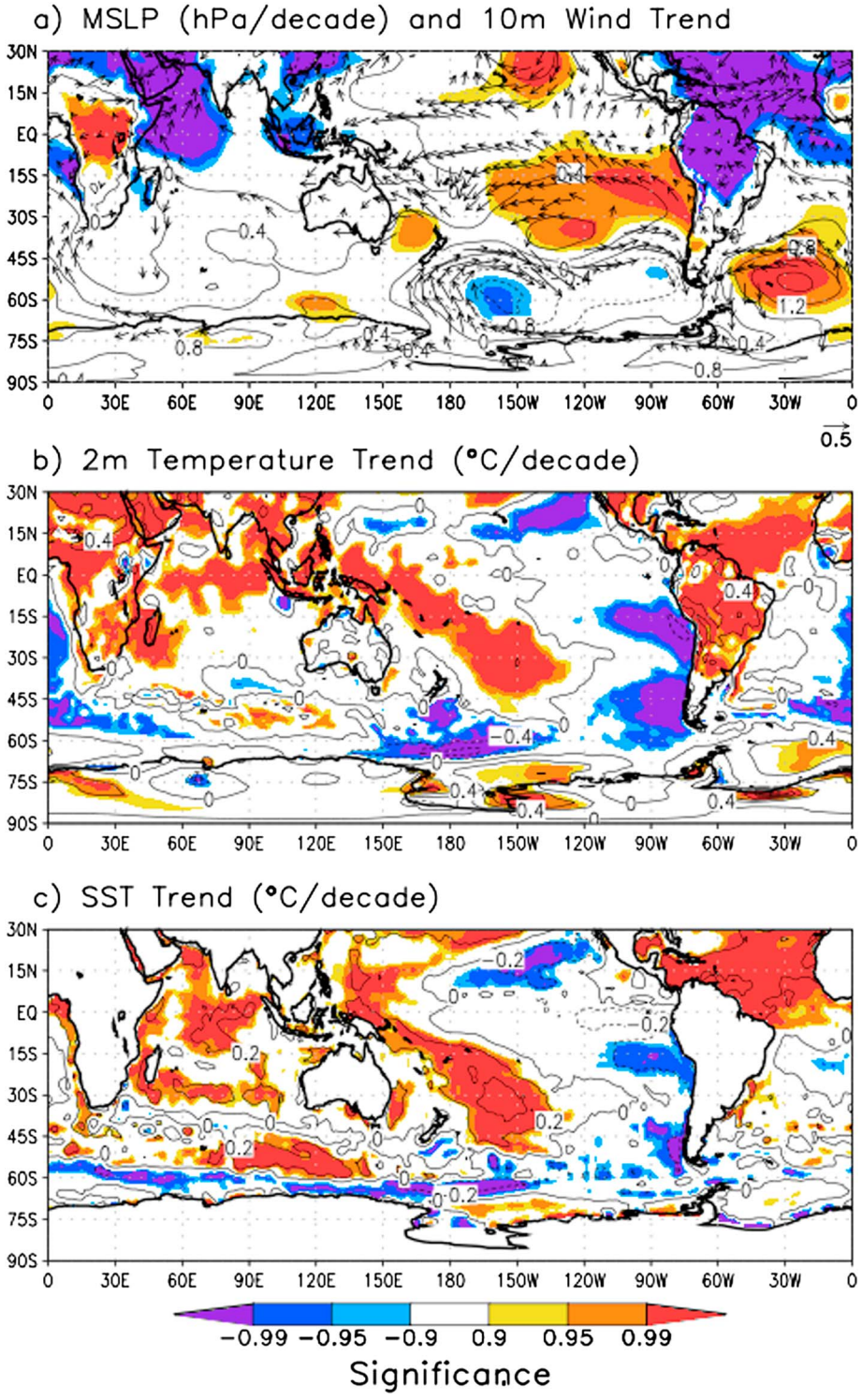

Figure 3. SON trends of (a) ERA-Interim MSLP and 10 m wind, 1979–2012, (b) ERA-Interim 2 m temperature, 1979–2012, and (c) NOAA OI SSTs, 1982–2012. Shading (from lightest to darkest) indicates regions where trends are statistically different from zero at $p < 0.10$, $p < 0.05$, and $p < 0.01$, respectively. Contour intervals for trends are indicated by plot headings; 10 m wind trends (in ms^{-1} $decade^{-1}$, indicated by reference vector) are only shown if at least one of the components has a significant trend different than zero at $p < 0.10$.

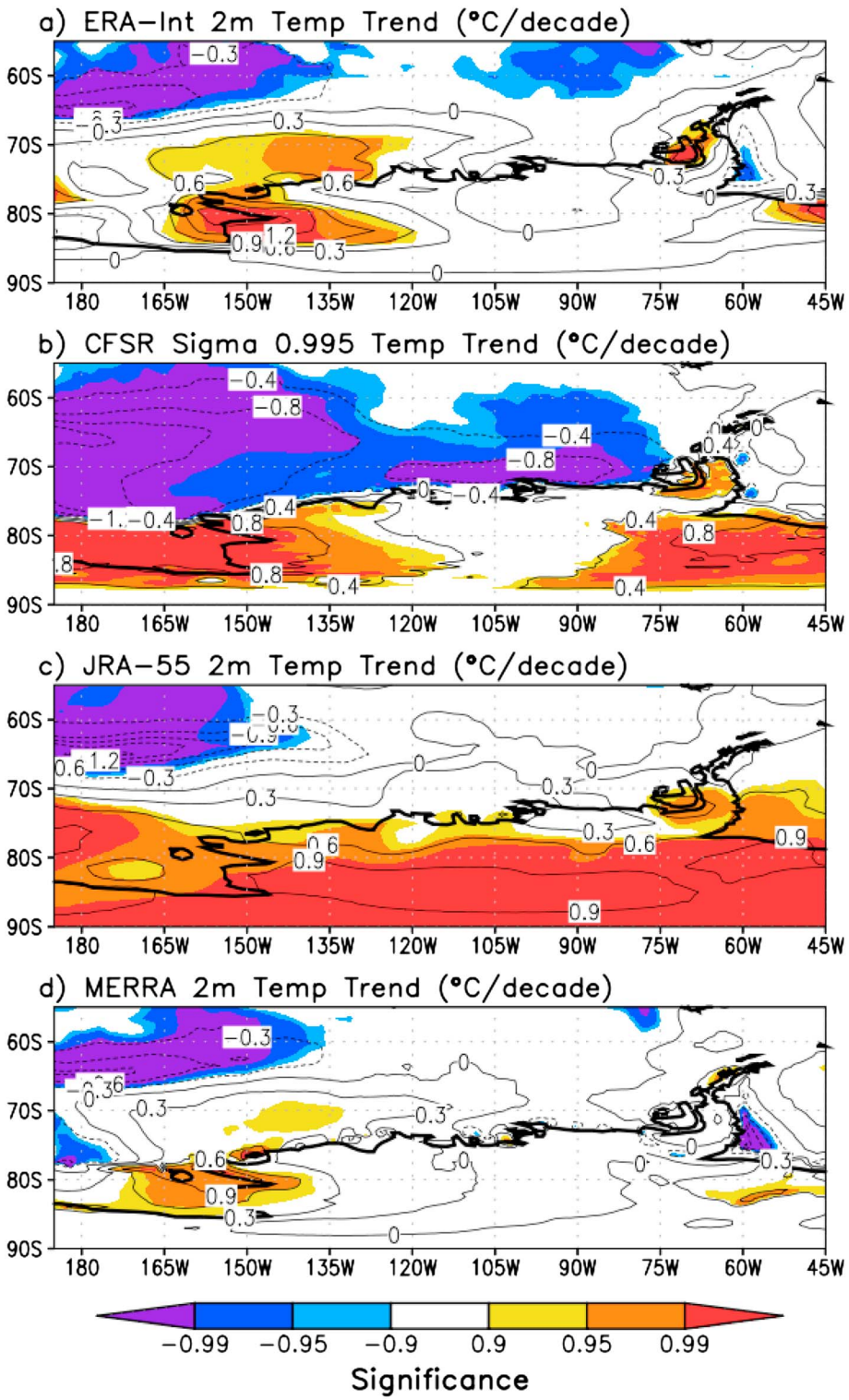

Figure 4. Near-surface SON temperature trends (in °C decade^{-1}) during 1979–2012 across West Antarctica and the Antarctic Peninsula. Shading indicates statistically significant trends as in Figure 3. (a) ERA-Interim 2 m temperatures, (b) CFSR sigma 0.995 level temperatures, (c) JRA-55 2 m temperatures, and (d) MERRA 2 m temperatures.

Table 3. The 1979–2012 SON Temperature Trends in Western West Antarctica (as in Figure 1 and Table 1) and a Modified Region Where Reanalysis Temperature Trends Are Most Similar in Figure 4 (76.5°–85.5°S, 120°–156°W), First Column, in Units of °C Decade^{-1} for the Various Reanalyses[a]

	Temperature Trend	Congruent With SOI	Congruent With PDO_Residual
	Original Western West Antarctica Region (72°S–85.5°S, 115.5°W–156°W)		
ERA-Interim	0.63	−0.02 (*−3.2%*)	0.13 (*20.6%*)
CFSR	0.26	−0.08 (*−32.4%*)	0.09 (*35.4%*)
JRA-55	0.66	−0.03 (*−5.3%*)	0.17 (*25.9%*)
MERRA	0.31	−0.12 (*−37.8%*)	0.12 (*38.7%*)
	Modified Western West Antarctica Region (76.5°S–85.5°S, 120°W–156°W)		
ERA-Interim	0.86	0.04 (*5.0%*)	0.18 (*20.4%*)
CFSR	0.72	0.00 (*−0.7%*)	0.20 (*27.4%*)
JRA-55	0.78	−0.02 (*−2.0%*)	0.21 (*27.3%*)
MERRA	0.38	−0.12 (*−32.3%*)	0.13 (*35.5%*)

[a]Also given are the portion/percentage (in parentheses) of these temperature trends linearly congruent with the SOI (second column) and PDO_residual (third column).

geostrophic flow around the deepening of the Amundsen Sea low (Figure 3a). The increased easterly winds here may enhance ice compaction (during this time of annual sea ice retreat) toward the western West Antarctic coast through dynamic Ekman transport, creating more ice-free conditions in the Amundsen Sea, north of the coast, and is therefore consistent with the warming 2 m temperatures in ERA-Interim and SSTs near coastal West Antarctica (Figures 3b and 3c). In this regard, the wind trends are consistent with the linkages between the local sea ice extent and inland West Antarctic warming discussed by *Schneider et al.* [2012]. Overall, the northerly wind trends north of coastal western West Antarctica (east and southeast of the deepening Amundsen Sea low) are consistent with the regional warming along at least coastal western West Antarctica and the SSTs there (Figures 3b and 3c).

To further quantify the differences among the reanalyses on the West Antarctic warming, Table 3 presents linear congruency between western West Antarctic temperatures for all four reanalyses (Figure 4) and the SOI and PDO_residual (as in Table 2). In the western West Antarctic region defined based on ERA-Interim, there are some differences in the temperature trends among reanalyses, as discussed in more detail by *Nicolas and Bromwich* [2014]. However, even for these cases the percentage of trends congruent with the PDO_residual is similar between the reanalyses, and the distinction between the role of the SOI and PDO is even more marked in other reanalyses. When considering a region of significant warming that all reanalyses share (defined as 76.5°–85.5°S, 120°–156°W from Figure 4), the temperature trends are more similar among the reanalyses (first column, Table 3), with the exception of MERRA that demonstrates the warming is more confined to the Ross Ice Shelf rather than interior West Antarctica (Figure 4d). From Table 3, and consistent with Table 2, the SOI has a weak to opposite linear relationship with western West Antarctica temperatures, implying that the recent positive trend in the SOI would be expected to yield either near-zero temperature change or a slight cooling over western West Antarctica. In stark contrast, the recent negative trend in the PDO_residual is far more related to the western West Antarctic warming and is linearly congruent with 20–35% of the warming found in the reanalyses. Further, in both regions the percentage of warming congruent with the PDO_residual (third column, Table 3) is lowest for the ERA-Interim, suggesting that the PDO_residual congruency values in Table 2 and Figure 6 are the most conservative estimates. Therefore the influence of the PDO changes on the (area-averaged) West Antarctic warming is consistent and robust among several reanalysis data sets, despite their subtle warming differences [*Nicolas and Bromwich*, 2014].

To investigate the relationship between the atmospheric circulation changes and 2 m temperatures with the SOI and the PDO_residual index (the two climate modes significantly trending during SON), spatial linear congruency plots are displayed in Figures 5 and 6. These plots, like Tables 2 and 3, show the portion of the trends spatially that are linearly congruent with (or can be expected from) changes in the SOI and PDO_residual; the shading in Figures 5 and 6 represent the percentage of the statistically significant MSLP and 2 m temperature trends (in Figures 5a and 6a, respectively) that are congruent with the SOI and PDO_residual index.

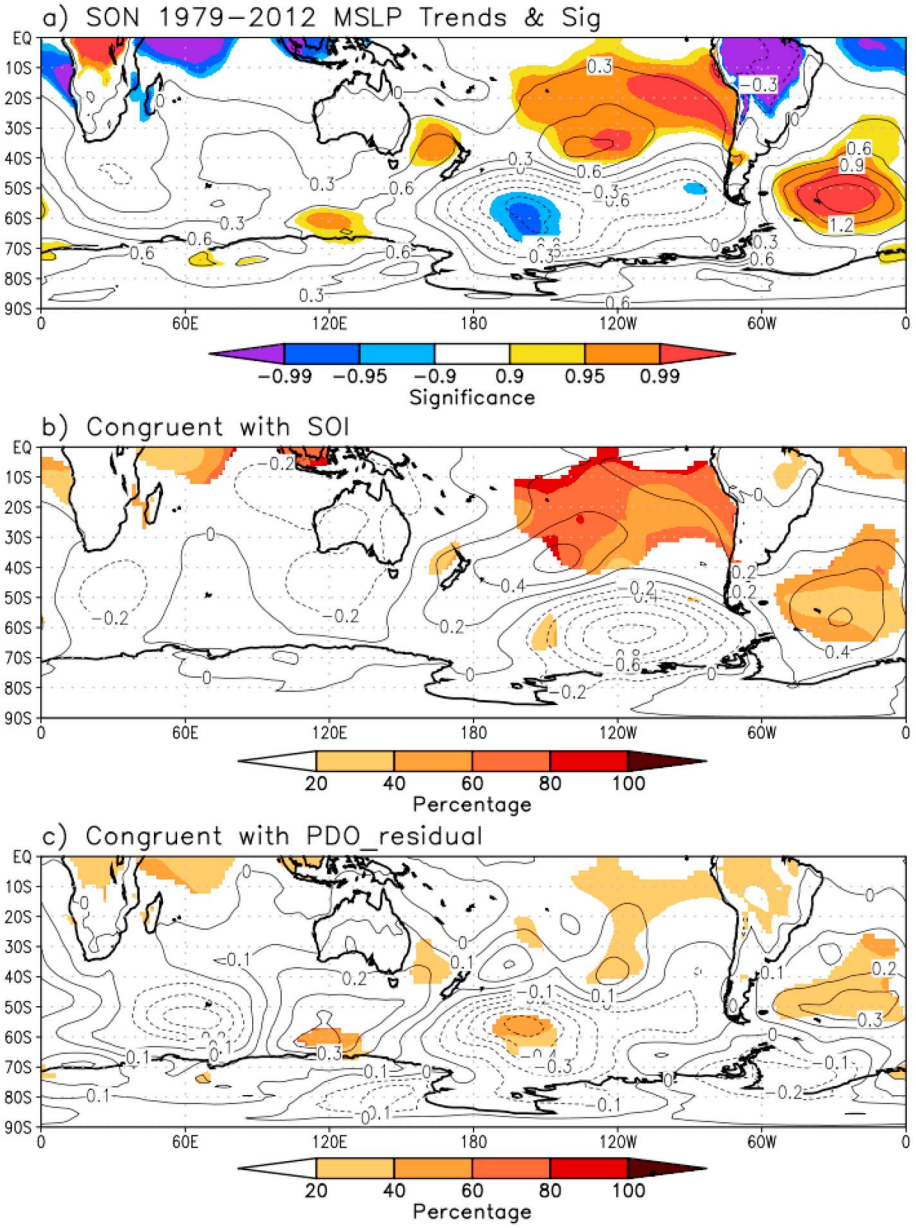

Figure 5. (a) Linear trends of SON ERA-Interim MSLP, 1979–2012, as in Figure 3a, (b) spatial linear congruency of the MSLP trends with the SOI, and (c) spatial linear congruency of the MSLP with the PDO_residual index. Shading in Figures 5b and 5c indicates percentage of the statistically significant trends in Figure 5a that are linearly congruent with the SOI and PDO_residual index, respectively.

Figure 5 shows that the increasing pressure in the South Atlantic is more strongly influenced by the SOI (on the order of 30–60% of the trend is congruent with the SOI), with a smaller influence from the PDO (20–30%). However, the deepening of the Amundsen Sea low is more strongly linearly related to the changes in the PDO_residual (broad region of 40–60%) rather than the SOI (small region of 20–30%). Figures 5a and 5b demonstrate that the SOI trend toward increased La Niña-like states is driving significant increases in pressure in the southwest South Atlantic. This increasing pressure in the southwest South Atlantic, combined with the persistent SOI response that occurs in the Amundsen Sea [*Clem and Fogt*, 2013] (contours in Figure 5b), increases the pressure gradient across the Peninsula, which in turn drives increased warm air advection onto the western Peninsula. Similarly, the PDO shows a stronger relationship to the warming across western West Antarctica after 1979 than the SOI (Tables 2 and 3); thus, the fact that the PDO trends are

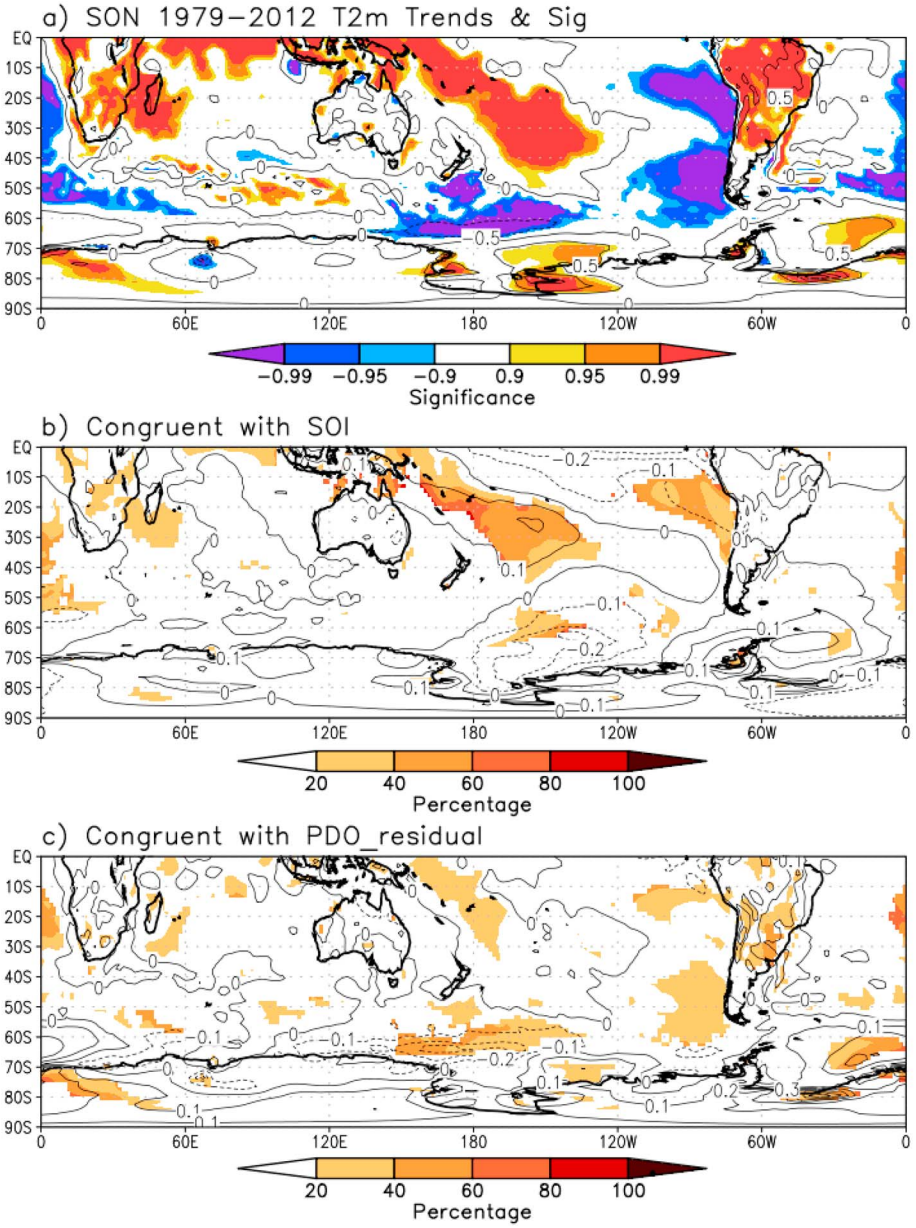

Figure 6. (a–c) As in Figure 5 but for the ERA-Interim 2 m temperature trends.

a stronger influence on the deepening of the Amundsen Sea low (Figure 5c) is also consistent with the PDO's influence on West Antarctic warming. Even if there is a strong causal link between the PDO_residual and SOI trends, Figure 5 clearly demonstrates that the PDO_residual and SOI trends are associated with different circulation changes across the Southern Hemisphere.

In terms of the 2 m temperature trends (Figure 6), again the tropical and subtropical trends are more strongly related to the changes in the SOI rather than the PDO. However, much of the cooling of the Southern Ocean is more strongly tied to the PDO, although the relationship is relatively modest (20–40% of the temperature trend is congruent). In the Ross Sea region, changes in both the PDO and SOI explain nearly equal magnitudes of the cooling there, while the PDO trend explains more of the significant warming along coastal West Antarctica and portions of interior West Antarctica (Figure 6c). These results confirm the area-averaged relationships found in Tables 2 and 3, which are even stronger in other reanalyses. In addition, 40–60% of the warming along the western Antarctic Peninsula is congruent with

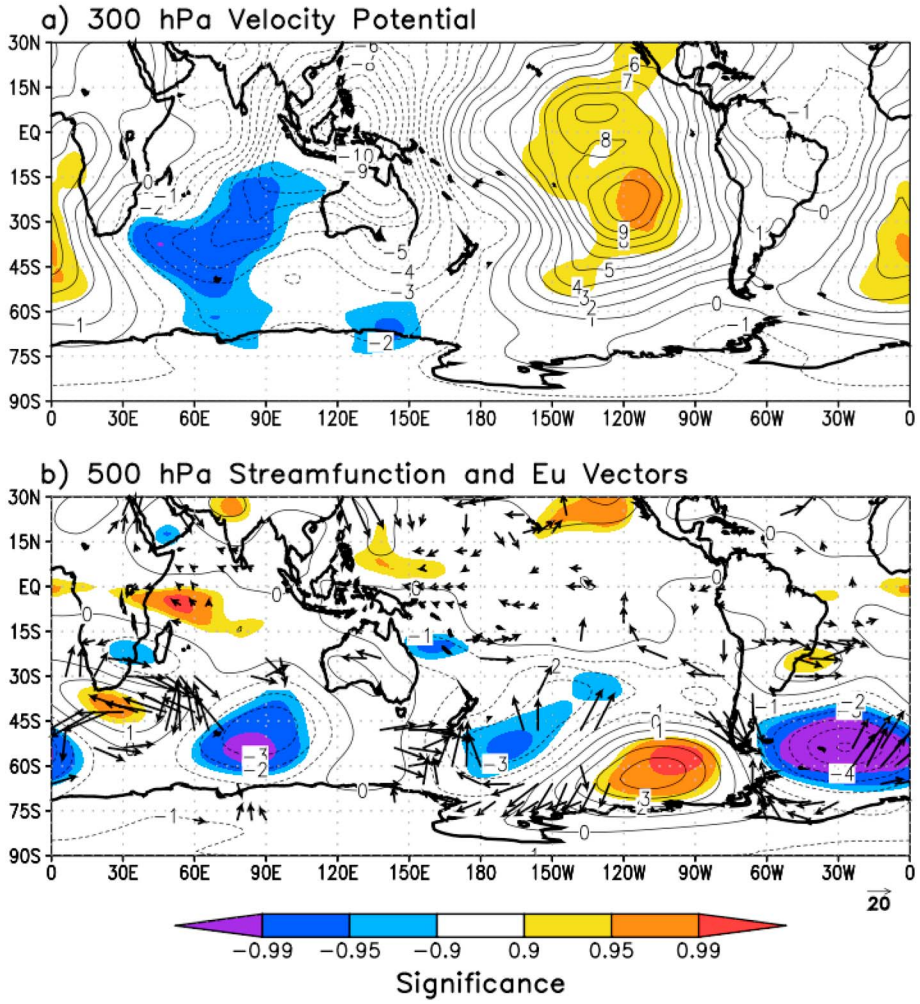

Figure 7. Anomaly composite mean for the top 6 highest years of pressure averaged in the South Atlantic region (45°–60°S, 45°–15°W) from 1979 to 2012 during SON. (a) ERA-Interim 300 hPa velocity potential anomalies and (b) ERA-Interim 500 hPa stream function anomalies and 300 hPa **Eu** vector anomalies. Shading (from lightest to darkest) indicates regions where the anomaly composite mean is statistically different from climatology at $p < 0.10$, $p < 0.05$, and $p < 0.01$, respectively. Contour intervals are 1×10^5 m^2 s^{-1} for Figure 7a and 1×10^6 m^2 s^{-1} for Figure 7b. **Eu** vector anomalies are only shown if at least one component is significantly different than climatology at $p < 0.10$.

the trend in the SOI (Figure 6b), also consistent with Table 2. As before, these results suggest different mechanisms tied to the warming along the western Antarctic Peninsula and western West Antarctica, in part related to the circulation changes of both the increased pressure in the South Atlantic and deepening of the Amundsen Sea low, respectively.

3.3. Forcing of the SON Atmospheric Circulation Changes

What is the explanation for these circulation changes? To answer this question, we investigate several diagnostic variables from ERA-Interim, namely, the 300 hPa velocity potential and 500 hPa stream function. Together, these fields will aid in depicting changes in the tropical divergence and the associated downstream response through atmospheric teleconnections. In order to better link the two processes, we also examine significant changes in Rossby wave propagation using the **Eu** vector formulation of *Trenberth* [1986, 1991]. This vector can be thought of as a localized Eliassen-Palm (E-P) flux and is therefore nearly equivalent to the E-P flux described by *Edmon et al.* [1980] or the barotropic version of the three dimensional Plumb flux [*Plumb*, 1986], although all ageostrophic terms are retained in its derivation. The zonal component of this vector is $\frac{1}{2}\left(\overline{v'^2 - u'^2}\right)$, while the meridional component is $\overline{-u'v'}$, the negative of the transient eddy momentum flux. Defined in this

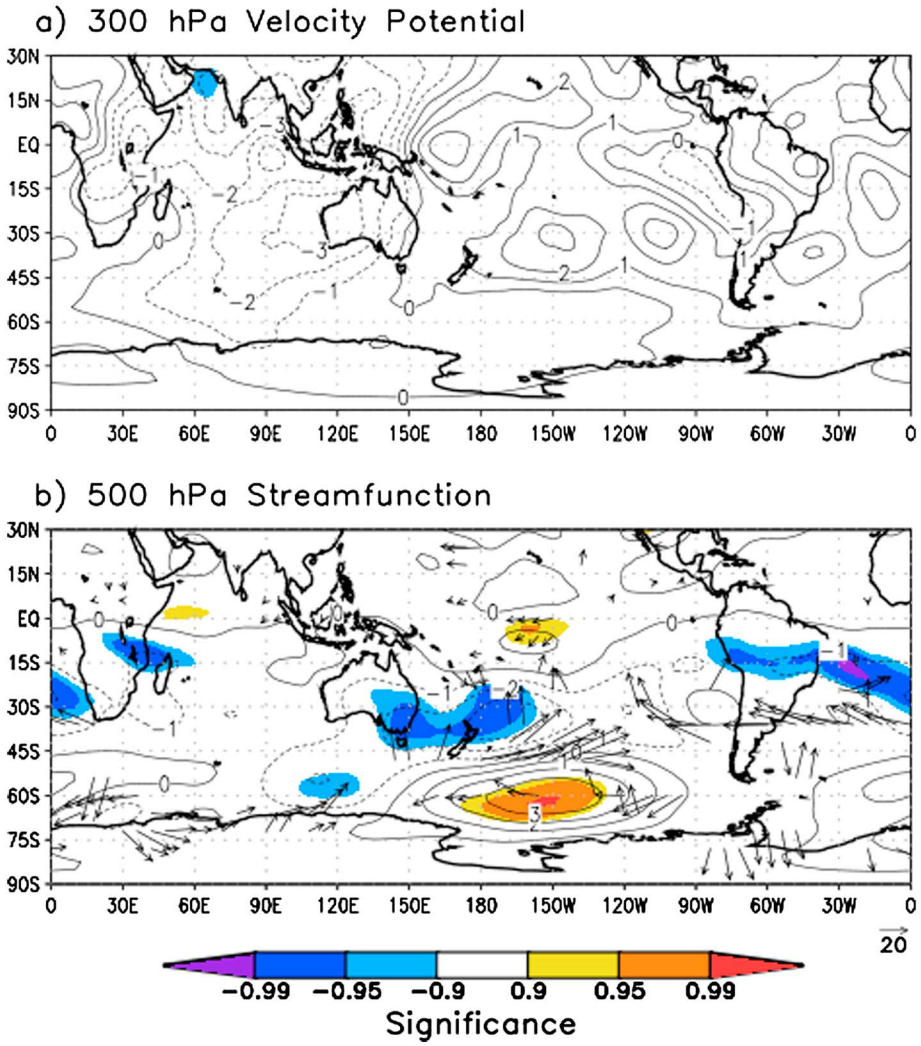

Figure 8. (a, b) As in Figure 7 but for the 6 years with the lowest pressure averaged in the Ross Sea region (54°–66°S, 165°–150°W).

fashion, **Eu** points in the direction of the relative group velocity of propagating Rossby waves, and its divergence represents a forcing on the westerly mean flow [*Trenberth*, 1991].

To investigate the tropical connections, anomaly composites were performed (Figures 7 and 8). Here we averaged the above variables over the 6 years with highest pressure area averaged in the South Atlantic, where pressure is trending positive (Figure 3a, 45°–60°S, 45°–15°W; Figure 7) and the 6 years with the lowest pressure in the eastern Ross Sea region, where pressure is trending negative (Figure 3a, 54°–66°S, 165°–150°W; Figure 8), and compared these averages to the 1981–2010 SON climatological average. Similar results are obtained using only 5 years, and except for the year 2008 (which both groups share), the two 6 year groups used for compositing are independent of each other. Shading (from lightest to darkest) indicates anomalies statistically different from zero at $p < 0.10$, $p < 0.05$, and $p < 0.01$. **Eu** vectors are only displayed in Figures 7 and 8 if at least one component is significantly different from climatology at $p < 0.10$.

The composites for the highest pressures in the South Atlantic region demonstrate a classic La Niña structure (Figure 7). In the 300 hPa velocity potential, an east-west couplet exists over the tropical Pacific, reflecting the Walker circulation: at 300 hPa, the significant positive velocity potential stretching from the central to eastern Pacific reflects above-average convergence at this level, or the potential for subsidence. Although not significant (likely due to the various location of convection in each La Niña event), the negative velocity potential over the western Pacific reflects divergence at 300 hPa and upward vertical motion. As discussed in

many previous studies [i.e., *Karoly*, 1989; *Revell et al*., 2001; *Lachlan-Cope and Connolley*, 2006], this pattern of divergence in the tropics drives a Rossby wave train that propagates through the South Pacific Ocean following a great circle trajectory, as indicated in the 500 hPa stream function composite (Figure 7b). Recall that in the Southern Hemisphere, due to the negative sign of the Coriolis parameter ($-f$), stream function anomalies are opposite in sign of geopotential height anomalies; thus, this Rossby wave train increases the pressures in the southwest South Atlantic (as expected) and decreases pressures in the Amundsen Sea (~115°W). Interestingly, although it is clear that this pattern is tropically forced, it is also evident that it operates relatively independent of the pressures in the eastern Ross Sea region (~160°W). By the 500 hPa stream function composite in Figure 7b, the Rossby wave train pattern driving the positive pressure trends in the South Atlantic would be associated with neutral to positive pressure trends in the Ross Sea region (Figure 7b), contrary to the negative pressure trends observed there (Figures 3a). This suggests that some additional forcing outside of that associated with the pressure trends in the South Atlantic is responsible for the negative pressure trends around 160°W. Further, the observed pressure trends in Figure 3a show no significant change in the central Amundsen Sea (~115°W) where we would expect a significant negative pressure trend to occur according to the stream function composite in Figure 7b. Therefore, the pressure trends found in the South Pacific (Figure 3a) are not directly associated with the pressure trends in the South Atlantic. In terms of the **Eu** vectors, there is a slight suggestion of an increased equatorward flux of wave activity throughout much of the tropical Pacific. Since the meridional component of the **Eu** vector is opposite in sign of the transient momentum flux, this in turn implies a more significant poleward momentum flux throughout the tropical Pacific, commonly observed during La Niña events [*L'Heureux and Thompson*, 2006; *Fogt et al*., 2011].

For years with low pressures in the eastern Ross Sea (Figure 8), there are no longer any significant velocity potential anomalies in the tropics, suggesting a stronger variance between the events or possibly pointing toward patterns operating on longer timescales (such as the PDO) that would not be as strongly evidenced in a composite over 6 years. Nonetheless, the mean velocity potential pattern displays a similar but weaker structure than in Figure 7, with a slight westward shift that places the zero line over the western Pacific rather than near the dateline (as in Figure 7). As such, this drives a notably different Rossby wave train that propagates more southerly from southeast Australia/New Zealand toward the Ross Sea (Figure 8b). While the **Eu** vectors show increased equatorward wave activity/poleward transient momentum fluxes throughout much of the Pacific, similar to Figure 7 and La Niña events [*L'Heureux and Thompson*, 2006; *Fogt et al*., 2011]; the most noteworthy feature is the more zonally oriented vectors near 45°S between the two stream function anomalies (Figure 8b). These **Eu** vectors represent the increased wave activity through the trough base of the deepened pressures/heights in the vicinity of the eastern Ross Sea, downstream of the ridge over southeast Australia/New Zealand. The **Eu** vectors strongly diverge in this region, which acts as a forcing mechanism for mean westerly flow. This is evidenced when looking at the 300 hPa zonal wind anomalies for the years with the lowest pressure in the eastern Ross Sea (Figure 9a), which shows a significant positive zonal wind anomaly southeast of New Zealand in the area of strongest **Eu** vector divergence. During years of high pressure in the South Atlantic, positive zonal wind anomalies are observed farther south and extend farther eastward across the midlatitude South Pacific, maximizing closer to the South American coast rather than in the western South Pacific. This scenario would help transport the Rossby wave activity across the South Pacific to the South Atlantic within the broader upper tropospheric westerly flow. From the composite difference (Figure 9c), it is clear that the upper tropospheric zonal winds during South Atlantic high-pressure years are significantly weaker in the midlatitudes of the western South Pacific near New Zealand, and significantly stronger in the eastern Ross Sea region and along the coast of western West Antarctica where there is significantly greater **Eu** divergence (Figure 7b).

Combining the 300 hPa zonal wind composites in Figure 9 with the **Eu** vectors in Figure 8b, it is suggested that during low-pressure years in the eastern Ross Sea region, the Rossby wave originating in the tropics ceases to propagate poleward and eastward as it encounters both the high terrain of Antarctica and the anomalously weak westerly flow near the West Antarctic coast. The Rossby wave in Figure 8b (Ross Sea low-pressure years) is also more meridionally structured than in Figure 7b (South Atlantic high-pressure years) with the midlatitude jet displaced farther equatorward toward New Zealand (Figures 9a and 9c). As such, the Rossby wave that drives the eastern Ross Sea low-pressure events likely becomes dissociated with the zonal background flow from the regional midlatitude jet (which acts as a waveguide for the propagation

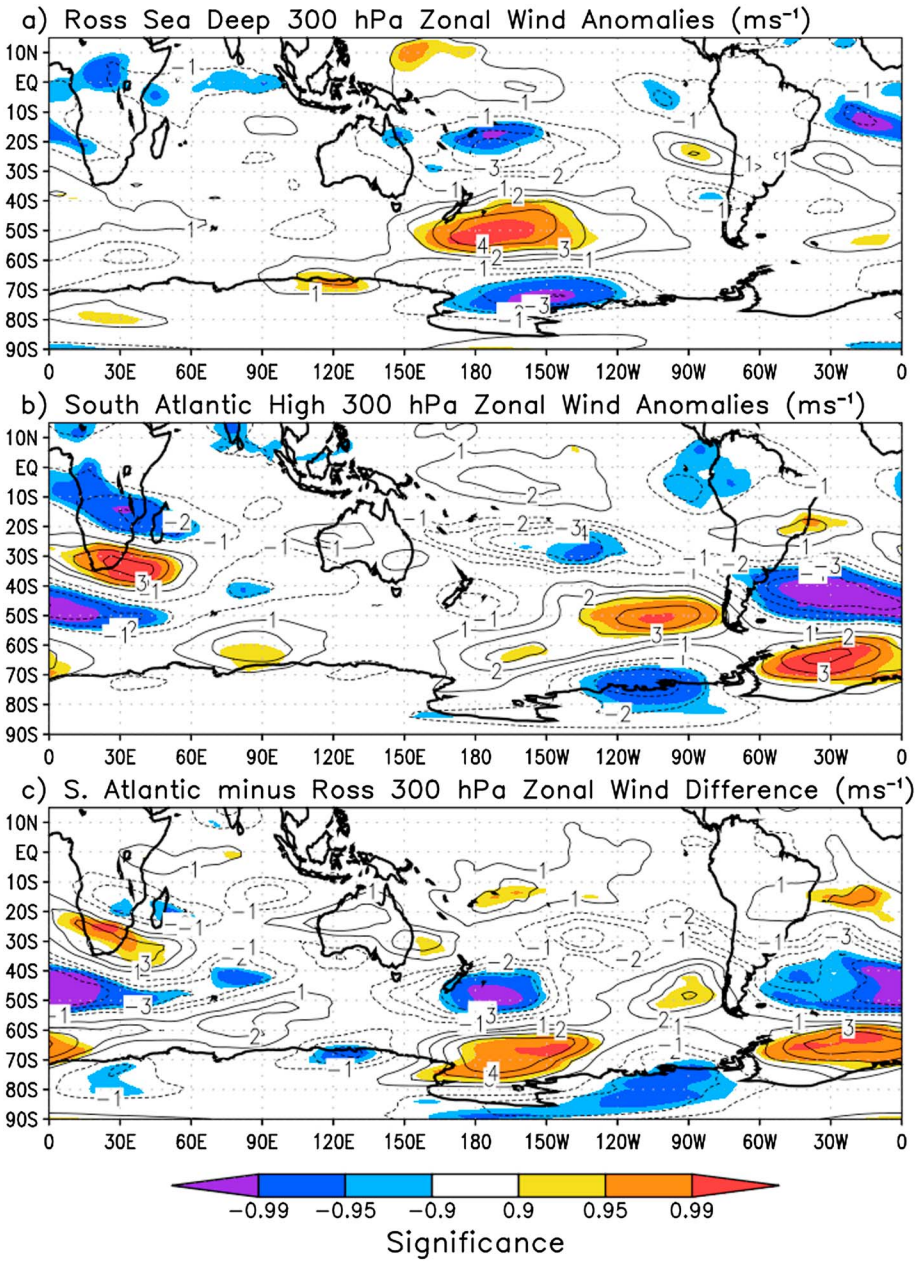

Figure 9. 300 hPa ERA-Interim zonal wind anomaly composites for (a) six lowest pressures in Ross Sea region, (b) six highest pressures in South Atlantic region, and (c) composite difference between Figures 9a and 9b. Shading indicates statistical significance of the anomalies or differences, as in Figure 7. Contour interval is 1 ms^{-1}.

depicted in Figure 8b) as it encounters anomalously strong westerly flow further north near New Zealand, thereby limiting its eastward propagation to the South Atlantic.

Although additional modeling and dynamical analysis beyond the scope of this paper is needed to fully confirm these hypotheses, we provide further evidence of different dynamic wave propagation as proposed above between the two composites in Figure 10. Here we present the 300 hPa velocity potential and **Eu** vector differences for the six lowest PDO_residual index years (trending negative and primarily congruent with the pressure changes in the Ross Sea region, Figure 5c) and the six highest SOI years (trending positive and primarily congruent with the pressure changes in the South Atlantic region, Figure 5b). Statistical significance of the difference is denoted by shading as in Figure 7, and only the **Eu** vectors with at least one

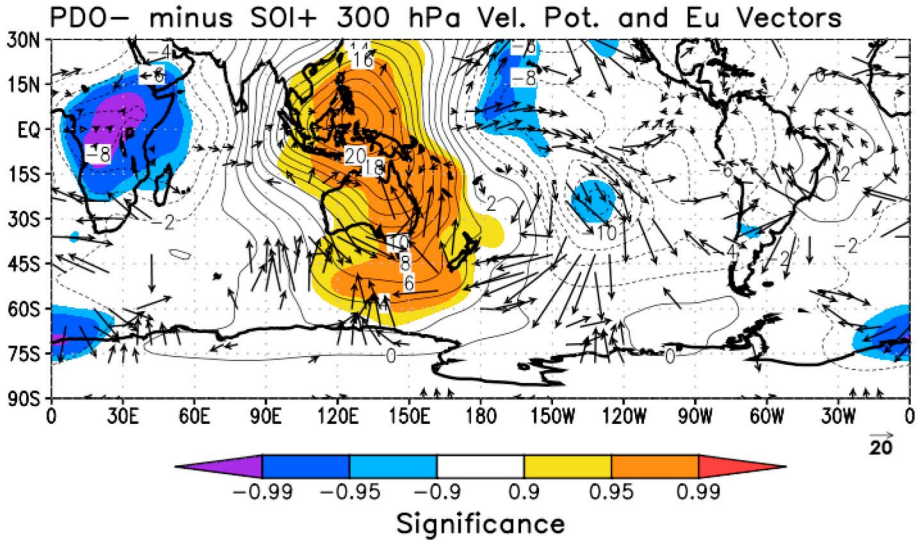

Figure 10. Composite difference between the six most negative PDO_residual years and the six most positive SOI years in SON, 1979–2012. Contours are the velocity potential (in 10^5 m^2 s^{-1}), with shading as in Figure 7. Also shown are the **Eu** vectors if at least one component is significantly different from zero at $p < 0.10$.

component being statistically different than zero at $p < 0.10$ are shown. As before, similar results are obtaining using a 5 year composite difference, and with the exception of the year 2011, the 6 years used for each group are independent of each other.

Clearly evident in the difference plot between these two climate modes (both producing La Niña-like characteristics and significantly trending) is the weakened velocity potential couplet in the tropical Pacific, in particular the reduced divergence/upward vertical motion over the western tropical Pacific. More prominent, however, is the different wave propagation structure between the two modes, which again highlights their connection to different circulation changes across the Southern Hemisphere. Compared to SOI positive/La Niña events, the negative PDO_residual years drive wave propagation emanating from the central tropical Pacific where there is increased divergence aloft/upward vertical motion (between the dateline and ~120°W), with a greater focus of wave activity toward the eastern Ross Sea rather than toward the central Amundsen Sea and downstream into the South Atlantic. In this design, the waves take a stronger meridional propagation, tied to the weaker poleward (more equatorward) momentum fluxes and 300 hPa jet configuration throughout the South Pacific. As such, the teleconnection takes a different structure, more closely resembling that in Figure 8, affecting only the eastern Ross Sea sector of the South Pacific. This explains the stronger connection between the deepening Amundsen Sea low and the negative PDO (or more precisely, the PDO trending negative), and the stronger connection of the pressures in the South Atlantic to the SOI positive/La Niña events.

Naturally, in the real world, these two features (La Niña and negative PDO events) are occurring simultaneously and cannot be separated statistically as is done in this analysis. Therefore, the total trend pattern in Figure 3a shows two centers of significant trends, while the trends in the central Amundsen Sea are insignificant due to a cancelation between the ENSO and PDO-related teleconnections (Figures 7b and 8b). Furthermore, the opposing circulation of these two modes in the central Amundsen Sea also likely explains why the statistical connections between the PDO and the western West Antarctic climate are more modest compared to the relationships between the SOI and western Antarctic Peninsula climate, as there is no cancelation in the South Atlantic (only the SOI teleconnection shows a significant response there, Figure 7b). By the same logic, this would also explain the lack of significant temperature trends across eastern West Antarctica after 1979; the opposing forcing from the PDO and ENSO make the pressure trends in this region weak (Figure 3a), thereby reducing the potential for significant temperature trends in the region between the Peninsula and western West Antarctica.

4. Discussion and Conclusions

This paper has examined in more detail the temperature and circulation trends across West Antarctica and the Antarctic Peninsula during SON. As suggested in previous work, only in SON are temperature trends across West Antarctica still statistically significant after 1979, and specifically only in the far western part of West Antarctica near the Siple coast. Our study examined how changes in the atmospheric circulation are related to these temperature trends and improves upon earlier work that suggested a primary link between autumn sea ice changes [*Ding and Steig*, 2013] or temperature trends across West Antarctica only [*Schneider et al*., 2012]

We note that increases in pressure in the South Atlantic have led to increased northerly flow over much of the northwest Antarctic Peninsula, consistent with the observed warming there, especially at Faraday and Rothera. The pressure increases are strongly linked to a trend toward more La Niña-like conditions inferred from a positive trend in the SOI and a negative trend in SSTs in the eastern tropical Pacific. Through changes in the upper atmospheric divergence across the tropics, this drives a wave train that propagates toward the Antarctic Peninsula, culminating in the South Atlantic, reminiscent of the Pacific-South American pattern [*Mo and Higgins*, 1998; *Mo and Paegle*, 2001]. Thus, circulation changes and sea ice changes [i.e., *Ding and Steig*, 2013] are both a contributing factor to the warming across the western Antarctic Peninsula in SON.

In contrast, the warming across western West Antarctica in SON after 1979 is more closely tied to a deepening of the Amundsen Sea low in the western Amundsen Sea/eastern Ross Sea. While there is increased northerly flow over the Amundsen Sea and South Pacific from this pressure trend, ERA-Interim 10 m wind trends near the West Antarctic coast are easterly, which when coupled with the wind trends farther north, could dynamically reduce sea ice in the region during its annual retreat and be associated with the warming (which is also evident in increasing SSTs off the coast of West Antarctica and consistent with results presented in *Schneider et al*. [2012]). The pressure trend toward a deeper Amundsen Sea low (and western West Antarctic warming) is more related to trends toward the negative polarity of the PDO compared to the positive trend in the SOI. Compared to typical La Niña events, the portions of the PDO variability linearly independent of ENSO show a weaker, but westward displaced pattern of convergence/divergence in the tropical Pacific, which drives a wave train that propagates more meridionally and terminates in the eastern Ross Sea. While this is broadly consistent with the tropical connections presented by *Schneider et al*. [2012], we have extended their analysis by showing a substantial portion of the circulation trend is more strongly tied to the PDO change rather than from PSA-like patterns. It thus remains to be seen if these circulation trends, and the associated warming and sea ice changes (both increases and decreases), will reverse when and if the PDO changes sign in the coming years.

While this work has increased the understanding of the statistical connections between the tropics and the extratropical Southern Hemisphere circulation changes, more work is needed. In particular, model simulations which dynamically demonstrate the mechanisms and their simultaneous forcing on the Southern Hemisphere circulation during austral spring are needed to better isolate the different ways the South Atlantic and eastern Ross Sea sector are responding to tropical variability. Modeling experiments can also help understand the likelihood that these circulation changes will continue into the future, especially those that examine the interactions between the ocean, ice, and atmosphere. Then, perhaps more predictions on the future rate and extent of warming across West Antarctica and the Antarctic Peninsula, and its global impact through sea level rise and changes in the ocean circulation, can be made.

Acknowledgments

Both authors acknowledge support from U.S. National Science Foundation, Office of Polar Programs through grant ANT-0944168. R.L.F. also acknowledges support from NSF grant ANT-1341621. ECMWF is thanked for providing the ERA-Interim data (accessed freely online at http://data-portal.ecmwf.int/data/d/interim_full_moda). NCEP is thanked for the CFSR data and the Japan Meteorological Agency is thanked for JRA-55 data (both accessed freely online at http://rda.ucar.edu/). The NASA Goddard Space Flight Center is thanked for the MERRA data (accessed freely online at http://disc.sci.gsfc.nasa.gov/). NOAA ESRL is thanked for the NOAA OI SST data (accessed freely online at http://www.esrl.noaa.gov/psd/data/gridded/data.noaa.oisst.v2.html). The Hadley Centre is thanked for providing the HadISST data for sea ice analysis (accessed freely online at http://www.metoffice.gov.uk/hadobs/hadisst/). Antarctic Peninsula temperature data were accessed freely online at http://www.antarctica.ac.uk/met/READER/data.html, the reconstructed Byrd station temperature record was accessed freely online at http://polarmet.osu.edu/Byrd_recon/, the Southern Oscillation Index (SOI) was accessed freely online through the Climate Prediction Center (http://www.cpc.ncep.noaa.gov/data/indices/), and the Pacific Decadal Oscillation (PDO) index was accessed freely online through the University of Washington at http://jisao.washington.edu/pdo/PDO.latest.

References

Bracegirdle, T. J., and G. J. Marshall (2012), The reliability of Antarctic tropospheric pressure and temperature in the latest global reanalyses, *J. Clim.*, *25*, 7138–7146.

Bromwich, D. H., J. P. Nicolas, and A. J. Monaghan (2011), An assessment of precipitation changes over Antarctica and the Southern Ocean since 1989 in contemporary global reanalyses, *J. Clim.*, *24*, 4189–4209.

Bromwich, D. H., J. P. Nicolas, A. J. Monaghan, M. A. Lazzara, L. M. Keller, G. A. Weidner, and A. B. Wilson (2013), Central West Antarctica among the most rapidly warming regions on Earth, *Nat. Geosci.*, *6*, 139–145, doi:10.1038/ngeo1671.

Bromwich, D. H., J. P. Nicolas, A. J. Monaghan, M. A. Lazzara, L. M. Keller, G. A. Weidner, and A. B. Wilson (2014), Corrigendum: Central West Antarctica among the most rapidly warming regions on Earth, *Nat. Geosci.*, *7*, 76, doi:10.1038/ngeo2016.

Chapman, W. L., and J. E. Walsh (2007), A synthesis of Antarctic temperatures, *J. Clim.*, *20*, 4096–4117.

Clem, K. R., and R. L. Fogt (2013), Varying roles of ENSO and SAM on the Antarctic Peninsula climate in austral spring, *J. Geophys. Res. Atmos.*, *118*, 11,481–11,492, doi:10.1002/jgrd.50860.

Dee, D. P., et al. (2011), The ERA-Interim reanalysis: Configuration and performance of the data assimilation system, *Q. J. R. Meteorol. Soc.*, *137*, 553–597.
Ding, Q., and E. J. Steig (2013), Temperature change on the Antarctic Peninsula linked to the tropical Pacific, *J. Clim.*, *26*, 7570–7585.
Ding, Q., E. J. Steig, D. S. Battisti, and M. Kuttel (2011), Winter warming in West Antarctica caused by central tropical Pacific warming, *Nat. Geosci.*, *4*, 398–403.
Ding, Q., E. J. Steig, D. S. Battisti, and J. M. Wallace (2012), Influence of the tropics on the Southern Annular Mode, *J. Clim.*, *25*, 6330–6348.
Edmon, H. J., B. J. Hoskins, and M. E. McIntyre (1980), Eliassen-Palm cross sections for the troposphere, *J. Atmos. Sci.*, *37*, 2600–2616.
Fogt, R. L., D. H. Bromwich, and K. M. Hines (2011), Understanding the SAM influence on the South Pacific ENSO teleconnection, *Clim. Dyn.*, *36*, 1555–1576.
Fogt, R. L., A. J. Wovrosh, R. A. Langen, and I. Simmonds (2012), The characteristic variability and connection to the underlying synoptic activity of the Amundsen-Bellingshausen Seas Low, *J. Geophys. Res.*, *117*, D07111, doi:10.1029/2011JD017337.
Garreaud, R. D., and D. S. Battisti (1999), Interannual (ENSO) and interdecadal (ENSO-like) variability in the Southern Hemisphere tropospheric circulation, *J. Clim.*, *12*, 2113–2123.
Holland, P. R., and R. Kwok (2012), Wind-driven trends in Antarctic sea-ice drift, *Nat. Geosci.*, *5*, 872–875.
Hosking, J. S., A. Orr, G. J. Marshall, J. Turner, and T. Phillips (2013), The influence of the Amundsen-Bellingshausen Seas Low on the climate of West Antarctica and its representation in coupled climate model simulations, *J. Clim.*, *26*, 6633–6648.
Jacobs, S. S., and J. C. Comiso (1997), Climate variability in the Amundsen and Bellingshausen Seas, *J. Clim.*, *10*, 697–709.
Karoly, D. J. (1989), Southern Hemisphere features associated with El Niño-Southern Oscillation events, *J. Clim.*, *2*, 1239–1252.
King, J. C. (1994), Recent climate variability in the vicinity of the Antarctic Peninsula, *Int. J. Climatol.*, *14*, 357–369.
Kobayashi, S., et al. (2015), The JRA-55 reanalysis: General specifications and basic characteristics, *J. Meteorol. Soc. Jpn.*, *93*, doi:10.2151/jmsj.2015-001.
Lachlan-Cope, T., and W. Connolley (2006), Teleconnections between the tropical Pacific and the Amundsen-Bellingshausen Seas: Role of the El Niño-Southern Oscillation, *J. Geophys. Res.*, *111* D23101, doi:10.1029/2005JD006386.
L'Heureux, M. L., and D. W. J. Thompson (2006), Observed relationships between the El-Niño-Southern Oscillation and the extratropical zonal-mean circulation, *J. Clim.*, *19*, 276–287.
Li, X., D. M. Holland, E. P. Gerber, and C. Yoo (2014), Impacts of the north and tropical Atlantic Ocean on the Antarctic Peninsula and sea ice, *Nature*, *505*, 538–542, doi:10.1038/nature12945.
Mantua, N. J., S. R. Hare, Y. Zhang, J. M. Wallace, and R. C. Francis (1997), A Pacific interdecadal climate oscillation with impacts on salmon production, *Bull. Am. Meteorol. Soc.*, *78*, 1069–1079.
Marshall, G. J. (2003), Trends in the southern annular mode from observations and reanalyses, *J. Clim.*, *16*, 4134–4143.
Marshall, G. J., A. Orr, N. P. M. van Lipzig, and J. C. King (2006), The impact of a changing Southern Hemisphere annular mode on Antarctic Peninsula summer temperatures, *J. Clim.*, *19*, 5388–5404.
Meredith, M. P., and J. C. King (2005), Rapid climate change in the ocean west of the Antarctic Peninsula during the second half of the 20th century, *Geophys. Res. Lett.*, *32*, C02S20, doi:10.1029/2005GL024042.
Mo, K. C., and R. W. Higgins (1998), The Pacific-South American modes and tropical convection during the Southern Hemisphere winter, *Mon. Weather Rev.*, *126*, 1581–1596.
Mo, K. C., and J. N. Paegle (2001), The Pacific-South American modes and their downstream effects, *Int. J. Climatol.*, *21*, 1211–1229.
Monaghan, A. J., D. H. Bromwich, W. Chapman, and J. C. Comiso (2008), Recent variability and trends of Antarctic near-surface temperature, *J. Geophys. Res.*, *113*, D04105, doi:10.1029/2007JD009094.
Nicolas, J. P., and D. H. Bromwich (2014), New reconstruction of Antarctic near-surface temperatures: Multidecadal trends and reliability of global reanalyses, *J. Clim.*, *27*, 8070–8093, doi:10.1175/JCLI-D-13-00733.1.
O'Donnell, R., N. Lewis, S. McIntyre, and J. Condon (2011), Improved methods for PCA-based reconstructions: Case study using the Steig et al. (2009) Antarctic temperature reconstruction, *J. Clim.*, *24*, 2099–2115.
Orr, A., G. J. Marshall, J. C. R. Hunt, J. Sommeria, C.-G. Wang, N. P. M. van Lipzig, D. Cresswell, and J. C. King (2008), Characteristics of summer airflow over the Antarctic Peninsula in response to recent strengthening of westerly circumpolar winds, *J. Atmos. Sci.*, *65*, 1396–1413.
Plumb, R. A. (1986), Three-dimensional propagation of transient quasi-geostrophic eddies and its relationship with the eddy forcing of the time-mean flow, *J. Atmos. Sci.*, *43*, 1657–1678.
Rayner, N. A., D. E. Parker, E. B. Horton, C. K. Folland, L. V. Alexander, D. P. Rowell, E. C. Kent, and A. Kaplan (2003), Global analyses of sea surface temperature, sea ice, and night marine air temperature since the late nineteenth century, *J. Geophys. Res.*, *108*(D14), 4407, doi:10.1029/2002JD002670.
Revell, M. J., J. W. Kidson, and G. N. Kiladis (2001), Interpreting low-frequency modes of Southern Hemisphere atmospheric variability as the rotational response to divergent forcing, *Mon. Weather Rev.*, *127*, 2233–2247.
Reynolds, R. W., N. A. Rayner, T. M. Smith, D. C. Stokes, and W. Wang (2002), An improved in situ and satellite SST analysis for climate, *J. Clim.*, *15*, 1609–1625.
Rienecker, M. M., et al. (2011), MERRA: NASA's Modern-Era Retrospective Analysis for Research and Applications, *J. Clim.*, *24*, 3624–3648, doi:10.1175/JCLI-D-11-00015.1.
Saha, S., et al. (2010), The NCEP climate forecast system reanalysis, *Bull. Am. Meteorol. Soc.*, *91*, 1015–1057, doi:10.1175/2010BAMS3001.1.
Schneider, D. P., C. Deser, and Y. Okumura (2012), An assessment and interpretation of the observed warming of West Antarctica in the austral spring, *Clim. Dyn.*, *38*, 323–347.
Schneider, N., and B. D. Cornuelle (2005), The forcing of the Pacific Decadal Oscillation, *J. Clim.*, *18*, 4355–4373.
Stammerjohn, S. E., D. G. Martinson, R. C. Smith, X. Yuan, and D. Rind (2008), Trends in Antarctic annual sea ice retreat and advance and their relation to El Niño-Southern Oscillation and Southern Annular Mode variability, *J. Geophys. Res.*, *113*, C03S90, doi:10.1029/2007JC004269.
Stammerjohn, S. E., R. Massom, D. Rind, and D. Martinson (2012), Regions of rapid sea ice change: An inter-hemispheric comparison, *Geophys. Res. Lett.*, *39*, L06501, doi:10.1029/2012GL050874.
Steig, E. J., D. P. Schneider, S. D. Rutherford, M. E. Mann, J. C. Comiso, and D. T. Shindell (2009), Warming of the Antarctic ice-sheet surface since the 1957 International Geophysical Year, *Nature*, *457*, 459–462, doi:10.1038/nature07669.
Thompson, D. W. J., J. M. Wallace, and G. C. Hegerl (2000), Annular modes in the extratropical circulation: Part II. Trends, *J. Clim.*, *13*, 1018–1036.
Trenberth, K. E. (1986), An assessment of the impact of transient eddies on the zonal flow during a blocking episode using localized Eliassen-Palm flux diagnostics, *J. Atmos. Sci.*, *43*, 2070–2087.
Trenberth, K. E. (1991), Storm tracks in the Southern Hemisphere, *J. Atmos. Sci.*, *48*, 2159–2178.
Trenberth, K. E., J. T. Fasullo, G. Branstator, and A. S. Phillips (2014), Seasonal aspects of the recent pause in surface warming, *Nat. Clim. Change*, *4*, 911–916, doi:10.1038/nclimate2341.

Turner, J., S. R. Colwell, G. J. Marshall, T. A. Lachlan-Cope, A. M. Carleton, P. D. Jones, V. Lagun, P. A. Reid, and S. Iagovkina (2004), The SCAR READER Project: Toward a high-quality database of mean Antarctic meteorological observations, *J. Clim.*, *17*, 2890–2898.

Turner, J., S. R. Colwell, G. J. Marshall, T. A. Lachlan-Cope, A. M. Carleton, P. D. Jones, V. Lagun, P. A. Reid, and S. Iagovkina (2005), Antarctic climate change during the last 50 years, *Int. J. Climatol.*, *25*, 279–294.

Turner, J., T. Phillips, J. S. Hosking, G. J. Marshall, and A. Orr (2013), The Amundsen Sea low, *Int. J. Climatol.*, *33*, 1818–1829.

Vaughan, D. G., G. J. Marshall, W. M. Connolley, C. Parkinson, R. Mulvaney, D. A. Hodgson, J. C. King, C. J. Pudsey, and J. Turner (2003), Recent rapid regional climate warming on the Antarctic Peninsula, *Clim. Change*, *60*, 243–274.

Zhang, Y., J. M. Wallace, and D. S. Battisti (1997), ENSO-like interdecadal variability: 1900–93, *J. Clim.*, *10*, 1004–1020.